# An Analysis of Small-Signal Substrate Resistance Effect in Deep-Submicrometer RF MOSFETs

Yo-Sheng Lin, *Member, IEEE,* and Shey-Shi Lu, *Senior Member, IEEE*

***Abstract*—Two different explanations of the $S_{22}$ kink phenomenon in deep-submicrometer RF MOSFETs have been reported in the Hjelmgren and Litwin attributed the phenomenon to the substrate resistance, while Lu *et al.* concluded that it results from the transconductance, or simply speaking, the size of the transistor. In this paper, we extend the dual-feedback circuit methodology for the three-terminal FET model proposed by Lu *et al.* into a more general four-terminal model in order to account for the influence of the substrate resistance. Our results show that, for a given MOSFET, either substrate resistance or transconductance may cause a kink in $S_{22}$. In addition to the single kink, which results from the above two factors, the double kinks, which appear when the substrate resistance of a MOSFET is within a middle range (approximately $10^2$ to $10^4$ $\Omega$), can also be accounted for by our extended model. Experimental data representative of 0.25-$\mu$m-gate MOSFETs are adopted to verify our theory. Excellent agreement between theoretical values and experimental data has been found, which indicates our theory can successfully explain the $S_{22}$ kink phenomenon in deep-submicrometer RF MOSFETs.**

***Index Terms*—Deep submicrometer, kink phenomenon, MOSFETs, substrate resistance.**

## I. Introduction

A COMPLETE understanding of the various phenomena that influence the $S$-parameters is one of the major prerequisites for achieving fully scalable models of deep-submicrometer RF MOSFETs. However, a behavior such as the kink phenomenon (anomalous dip) in the scattering parameter $S_{22}$ of RF MOSFETs with high substrate resistance, as reported by Hjelmgren and Litwin [1], is not well explained. For instance, to begin with, in [1], the measured frequency at which the kink phenomenon appeared was low ($<$1 GHz), while the simulated frequency at which the kink phenomenon appeared was high ($>$5 GHz). The authors seemed to regard these two kinks as the same type, which is problematic. It will be explained in Section IV that the measured and simulated kinks belong to different types of kinks. In addition, in [1], it is strange that the kink phenomenon was invisible when the substrate resistance was small, but became apparent when the substrate resistance of a MOSFET was in the order of $10^2$ to $10^3$ $\Omega$. Hjelmgren and Litwin did not explain this phenomenon deeply based on device physics. It will also be explained in Section IV that the observed kink phenomenon is due to the intrinsic triple characteristic of the output impedance of the MOSFETs.

Besides, Lu *et al.* reported that the kink phenomenon could be caused by a relatively larger transconductance or, simply speaking, a relatively larger size of the FET [2]. The frequency at which such a kink phenomenon appeared was high ($>$5 GHz).

Therefore, in this paper, we would like to study the correlation between these observed kink phenomena reported in [1] and [2], and to investigate how substrate resistance influences the number of kinks and their corresponding frequencies based on both theoretical analysis and measurement data. In order to achieve these goals, a theory for four-terminal MOSFETs based on the Lu *et al.* theory for three-terminal FETs has been developed. Lu *et al.* propose a theory based on dual-feedback circuit methodology to explain why the kink phenomenon of the scattering parameter $S_{22}$ is usually found in three-terminal FETs of larger sizes, and why it is much easier to see the kink phenomenon in bipolar transistors rather than in three-terminal FETs [2], [3]. On the basis of their theory, we create a more general four-terminal model by adding a substrate network to account for the influence of the substrate resistance. The kink phenomenon of the scattering parameter $S_{22}$ of deep-submicrometer RF MOSFETs with high substrate resistance is explained by deriving the output impedance (or admittance) of a four-terminal MOSFET under the measurement conditions of $S$-parameters. By observing the behaviors of the output impedance (or admittance) at both high and low frequencies, the kink phenomenon can be easily explained. Moreover, to further verify this approach, we also applied the above method to obtain the other three $S$-parameters, i.e., $S_{11}$, $S_{21}$, and $S_{12}$, and compared them with our experimental data. Excellent agreement between theoretical values and experimental data has been found from these comparisons.

## II. Theory

Now, consider the circuit shown in Fig. 1(a), where a MOSFET is connected for measuring its $S$-parameters. $S_{11}$ and $S_{21}$ can be measured by setting $V_2 = 0$ and $V_1 \neq 0$, while $S_{22}$ and $S_{12}$ can be measured by setting $V_1 = 0$ and $V_2 \neq 0$. The small-signal model parameters were extracted from the measured $S$-parameters based on the direct extraction methods introduced in [4] and [5]. In general, the circuit in Fig. 1(a) is hard to handle. However, the problem will be much easier to solve if the circuit is viewed as a dual-feedback circuit [6]. In order to simplify the circuit analysis, we temporarily neglect all the inductors in Fig. 1(a). Actually, the effects of the inductors are negligible. Based on the extracted small-signal model parameters of an nMOSFET with gate length of 0.25-$\mu$m,

Manuscript received July 11, 2002; revised December 9, 2002. This work was supported by the National Science Council of the R.O.C. under Contract NSC91-2218-E-260-006 and Contract NSC91-2218-E-002-018.

Y.-S. Lin is with the Department of Electrical Engineering, National Chi-Nan University, Puli, Taiwan, R.O.C. (e-mail: stephenlin@ncnu.edu.tw).

S.-S. Lu is with the Department of Electrical Engineering and Institute of Electronics, National Taiwan University, Taipei, Taiwan, R.O.C.

Digital Object Identifier 10.1109/TMTT.2003.810135

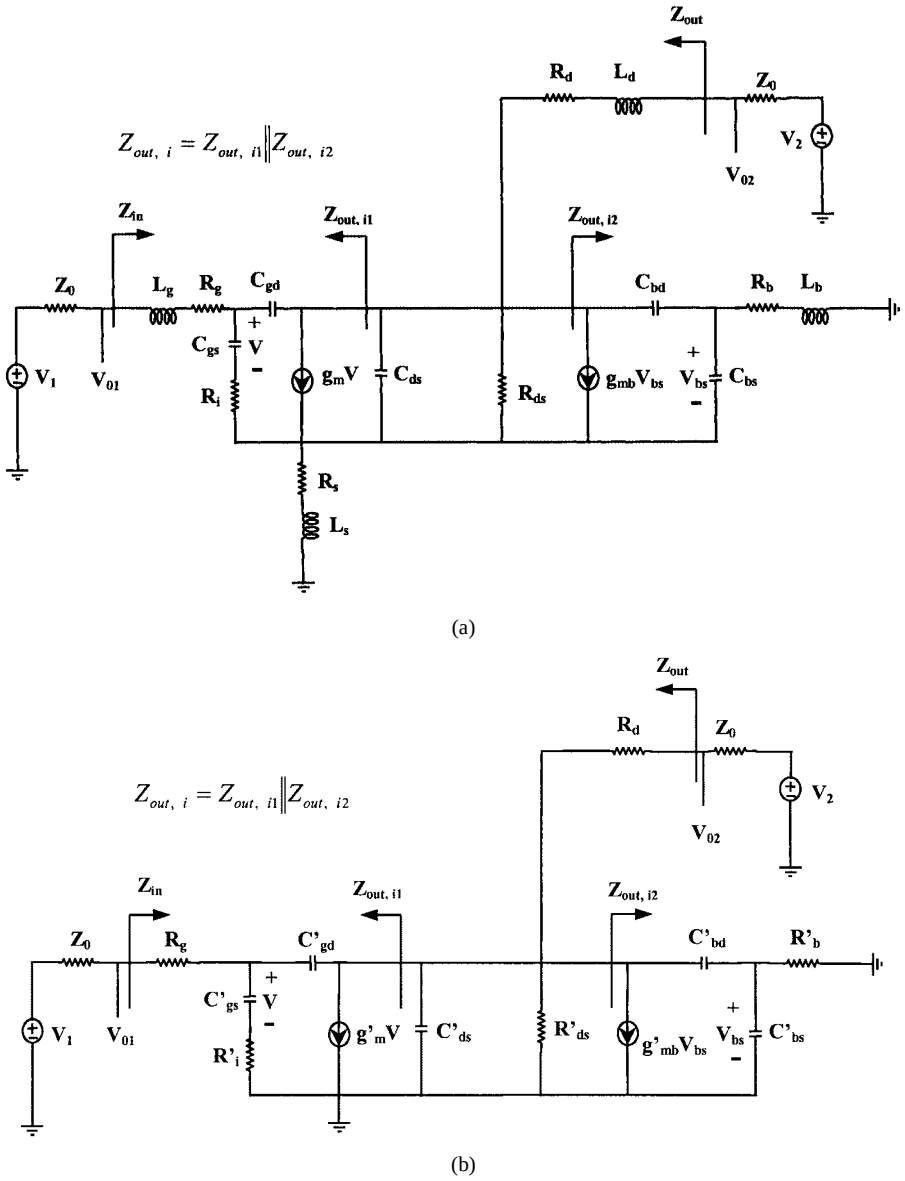


Fig. 1. Setup for the measurement of MOSFETs $S$-parameters including body terminal. (a) A complete circuit including extracted equivalent-circuit parameters of a 0.25-$\mu$m-gate Si nMOSFET with gate length of 80 $\mu$m and substrate resistance of 250.3 $\Omega$. (b) A simplified circuit with the local series–series feedback element ($R_s$) absorbed.

gatewidth of 80 $\mu$m, and extracted substrate resistance of 250.3 $\Omega$, the magnitude of the impedance of $L_g$, $L_s$, $L_d$, and $L_b$ at the frequency of 20 GHz is 0.31, 0.11, 0.24, and 0.13 $\Omega$, respectively, below the 10% of their corresponding resistance $R_g$, $R_s$, $R_d$, and $R_b$, which is 43.6, 1.2, 5.3, and 250.3 $\Omega$, respectively. In addition, although all the inductors are negligible in this study, they can be easily included in theoretical calculations in the cases when they are not negligible. We will discuss this in Section IV.

The circuit of Fig. 1(a) can be transformed into that of Fig. 1(b). In addition to [2, eqs. (2)–(7)], the additionally required circuit element modifications are as follows:

$$g'_{mb} = \frac{g_{mb}}{1 + g_m R_s} \tag{1}$$

$$C'_{bd} = \frac{C_{bd}}{1 + g_m R_s} \tag{2}$$

$$C'_{bs} = \frac{C_{bs}}{1 + g_m R_s} \tag{3}$$

$$R'_b = R_b(1 + g_m R_s) \tag{4}$$

where $g_{mb} = g_{mbo} \cdot \exp(-j\omega\tau)$, in which $g_{mbo}$ stands for the dc transconductance. Meanwhile, all the other symbols retain their usual meaning. The right-hand side of $R'_{\rm ds}$ (or $R_{\rm ds}$) can be regarded as a circuit element with impedance $Z_{{\rm out},\,i2}$. From (1)–(4), it can be shown that $Z_{{\rm out},\,i2}$ in Fig. 1(b) is equal to $Z_{{\rm out},\,i2}$ in Fig. 1(a) multiplied by $(1 + g_m R_s)$, which is consistent with the local series–series feedback theory adopted here [6].

If the expression for the output impedance $Z_{\rm out}$ of Fig. 1(b) has been found, then $S_{22}$ is given by

$$S_{22} = \frac{Z_{\rm out} - Z_O}{Z_{\rm out} + Z_O}. \tag{5}$$

For the convenience of the discussion about the origin of the kink phenomenon of the scattering parameter $S_{22}$ of deep-submicrometer RF MOSFETs with high substrate resistance, we define an "intrinsic output impedance" $Z_{\mathrm{out},i}$ as

$$Z_{\mathrm{out},i} = Z_{\mathrm{out},i1} \| Z_{\mathrm{out},i2} \tag{6}$$

where the symbol $\|$ represents parallel combination. $Z_{\mathrm{out},i1}$ is the impedance seen to the left-hand side of the drain-to-source capacitance $C'_{\mathrm{ds}}$ (or $C_{\mathrm{ds}}$), while $Z_{\mathrm{out},i2}$ is the impedance seen to the right-hand side of the drain-to-source resistance $R'_{\mathrm{ds}}$ (or $R_{\mathrm{ds}}$). By intrinsic, we mean that this output impedance does not include $R_{\mathrm{ds}}$, $R_d$, and $C_{\mathrm{ds}}$, which is different from the normally defined output impedance $Z_{\mathrm{out}}$ seen to the left-hand side of $Z_O$ and $V_2$, as indicated in Fig. 1. The expressions of impedances $Z_{\mathrm{out},i1}$ and $Z_{\mathrm{out},i2}$ can then be derived from the local shunt–shunt theory [6] and are given by

$$\begin{aligned} Z_{\mathrm{out},i1} &= \frac{\left(sC''_{\mathrm{gs}} + \frac{1}{Z_{O1}}\right)^{-1} + \frac{1}{sC'_{\mathrm{gd}}}}{1 + g''_m\left(sC''_{\mathrm{gs}} + \frac{1}{Z_{O1}}\right)^{-1}} \\ &= \frac{1 + s\left(C''_{\mathrm{gs}} + C'_{\mathrm{gd}}\right)Z_{O1}}{(1 + g''_m Z_{O1})sC'_{\mathrm{gd}} + s^2 C''_{\mathrm{gs}} C'_{\mathrm{gd}} Z_{O1}} \end{aligned} \tag{7}$$

and

$$\begin{aligned} Z_{\mathrm{out},i2} &= \frac{\left(sC'_{bs} + \frac{1}{R'_b}\right)^{-1} + \frac{1}{sC'_{bd}}}{1 + g'_{mb}\left(sC'_{bs} + \frac{1}{R'_b}\right)^{-1}} \\ &= \frac{1 + s(C'_{bs} + C'_{bd})R'_b}{\left(1 + g'_{mb}R'_b\right)sC'_{bd} + s^2 C'_{bs} C'_{bd} R'_b} \end{aligned} \tag{8}$$

where $C''_{\mathrm{gs}} = C'_{\mathrm{gs}}/(1 + sR'_i C'_{\mathrm{gs}})$, $g''_m = g'_m/(1 + sR'_i C'_{\mathrm{gs}})$, and $Z_{O1} = Z_O + R_g$. Once these two impedances are known, $Z_{\mathrm{out},i}$ is equal to the parallel combination of $Z_{\mathrm{out},i1}$ and $Z_{\mathrm{out},i2}$. The normal output impedance is the parallel combination of $Z_{\mathrm{out},i}$, $C'_{\mathrm{ds}}$, and $R'_{\mathrm{ds}}$ followed by a series combination with $R_d$ as follows:

$$Z_{\mathrm{out}} = \left(Z_{\mathrm{out},i} \left\| \frac{1}{sC'_{\mathrm{ds}}} \right\| R'_{\mathrm{ds}}\right) + R_d. \tag{9}$$

From (9), $S_{22}$ can be determined according to (5).

In order to analyze the small-signal substrate resistance effect on the scattering parameter $S_{22}$ of deep-submicrometer RF MOSFETs, (6) for the intrinsic output impedance has to be reexamined more closely. To give more insights into (6), let us assume that $R'_i$ is negligibly small, which is usually the case. Therefore, the general behavior of (6) will not be affected much by neglecting $R'_i$. Under this assumption, (6) is equal to

$$\begin{aligned} Z_{\mathrm{out},i} = &\left(\frac{1 + s\left(C'_{\mathrm{gs}} + C'_{\mathrm{gd}}\right)Z_{O1}}{(1 + g'_m Z_{O1})sC'_{\mathrm{gd}} + s^2 C'_{\mathrm{gs}} C'_{\mathrm{gd}} Z_{O1}}\right) \\ &\left\| \left(\frac{1 + s(C'_{bs} + C'_{bd})R'_b}{\left(1 + g'_{mb}R'_b\right)sC'_{bd} + s^2 C'_{bs} C'_{bd} R'_b}\right)\right. . \end{aligned} \tag{10}$$

After inserting $s = j\omega$ into (10) and after some simple mathematical manipulations, we find that, at high frequencies, $Z_{\mathrm{out},i}$ can be approximated by a parallel *RC* network, while at low frequencies, when $R'_b \ll 1/|j\omega C'_{bs}|$ (which is usually the case), $Z_{\mathrm{out},i}$ can be approximated by a series *RC* network, i.e., at high frequencies

$$\begin{aligned} Y_{\mathrm{out},i} &= \frac{1}{Z_{\mathrm{out},i}} \\ &= \frac{1}{Z_{\mathrm{out},i1}} + \frac{1}{Z_{out,i2}} \\ &\approx \left[Y_{O1}\left(\frac{C'_{\mathrm{gd}}}{C'_{\mathrm{gs}} + C'_{\mathrm{gd}}}\right)^2 + g'_m \frac{C'_{\mathrm{gd}}}{C'_{\mathrm{gs}} + C'_{\mathrm{gd}}}\right] \\ &\quad + \left[Y'_b\left(\frac{C'_{bd}}{C'_{bs} + C'_{bd}}\right)^2 + g'_{mb}\frac{C'_{bd}}{C'_{bs} + C'_{bd}}\right] \\ &\quad + j\omega\left(\frac{C'_{\mathrm{gs}}C'_{\mathrm{gd}}}{C'_{\mathrm{gs}} + C'_{\mathrm{gd}}} + \frac{C'_{bs}C'_{bd}}{C'_{bs} + C'_{bd}}\right) \\ &\approx (g_1 + g_2) + s(C_{P1} + C_{p2}) \\ &\approx g + sC_P. \end{aligned} \tag{11}$$

While at low frequencies, when $R'_b \ll 1/|j\omega C'_{bs}|$

$$\begin{aligned} Z_{\mathrm{out},i} &= Z_{\mathrm{out},i1} \| Z_{\mathrm{out},i2} \\ &\approx \left(\frac{Z_{O1}}{1 + g'_m Z_{O1}} + \frac{g'_m}{(Y_{O1} + g'_m)^2} \times \frac{C'_{\mathrm{gs}}}{C'_{\mathrm{gd}}}\right) \\ &\quad \cdot \left(\frac{(1 + g'_m Z_{O1})C'_{\mathrm{gd}}}{(1 + g'_m Z_{O1})C'_{\mathrm{gd}} + (1 + g'_{mb}R'_b)C'_{bd}}\right)^2 \\ &\quad + \left(\frac{R'_b}{1 + g'_{mb}R'_b} + \frac{g'_{mb}}{(Y'_b + g'_{mb})^2} \times \frac{C'_{bs}}{C'_{bd}}\right) \\ &\quad \cdot \left(\frac{(1 + g'_{mb}R'_b)C'_{bd}}{(1 + g'_m Z_{O1})C'_{\mathrm{gd}} + (1 + g'_{mb}R'_b)C'_{bd}}\right)^2 \\ &\quad + \frac{1}{j\omega[(1 + g'_m Z_{O1})C'_{\mathrm{gd}} + (1 + g'_{mb}R'_b)C'_{bd}]} \\ &\approx r_1\left(\frac{C_{s1}}{C_{s1} + C_{s2}}\right)^2 + r_2\left(\frac{C_{s2}}{C_{s1} + C_{s2}}\right)^2 \\ &\quad + \frac{1}{j\omega(C_{s1} + C_{s2})} \approx r + \frac{1}{j\omega C_s} \end{aligned} \tag{12}$$

where $Y_{O1}$ and $Y'_b$ is the reciprocal of $Z_{O1}$ and $R'_b$, respectively. The results of (11) and (12) are reasonable from the physical point-of-view and can be qualitatively understood as follows. Compared with $C'_{\mathrm{gs}}$ and $C'_{bs}$, respectively, $Z_{O1}(=Z_O + R_g)$ and $R'_b$ can be regarded as open circuits at very high frequencies. The total capacitance is thus the parallel combination of the series combination of $C'_{\mathrm{gs}}$ and $C'_{\mathrm{gd}}$ and the series combination of $C'_{bs}$ and $C'_{bd}$. The current sources $g'_m V$ can be replaced by a conductance determined by the ratio of the $C'_{\mathrm{gs}}$ and $C'_{\mathrm{gd}}$ capacitive voltage divider, while $g'_{mb}V_{bs}$ can be replaced by a conductance determined by the ratio of the $C'_{bs}$ and $C'_{bd}$ capacitive voltage divider. Therefore, the circuit results in a parallel *RC* circuit. On the other hand, at low frequencies when $R'_b \ll 1/|j\omega C'_{bs}|$,

$C'_{\rm gs}$ and $C'_{bs}$ compared with $Z_{O1}$ and $R'_b$, respectively, can be viewed as open circuits. Thus, $Z_{O1}$ is in series with $C'_{\rm gd}$, while $R'_b$ is in series with $C'_{bd}$. It can be proven that the final result of the parallel combination of the two dependent current sources and the two series *RC* circuits is again a series *RC* circuit.

Note that an exceptional case of $Z_{{\rm out},\,i2}$ at low frequencies is when $R'_b \gg 1/|j\omega C'_{bs}|$. That is, $R'_b$ is far larger than the equivalent resistance of $C'_{bs}$ and can be treated as an open circuit. The total capacitance $C'_{s2}$ is thus the series combination of $C'_{bs}$ and $C'_{bd}$ or is equal to $C'_{bs}\cdot C'_{bd}/(C'_{bs}+C'_{bd})$. Moreover, the current source $g'_{mb}V_{bs}$ can be replaced by a resistance $r'_2$ equal to $(C'_{bs}+C'_{bd})/(C'_{bd}\cdot g'_{mb})$, which is determined by the ratio of the $C'_{bs}$ and $C'_{bd}$ capacitive voltage divider. It is noteworthy that, at high or at low frequencies, when $R'_b \gg 1/|j\omega C'_{bs}|$, the $Z_{{\rm out},\,i2}$ of the two conditions can both be represented by a parallel *RC* network. The corresponding resistances are consistent, i.e., $1/g_2 = Y'_b(C'_{bd}/(C'_{bs}+C'_{bd}))^2 + g'_{mb}C'_{bd}/(C'_{bs}+C'_{bd})$ and $r'_2 = (C'_{bs}+C'_{bd})/(C'_{bd}\cdot g'_{mb})$, thus, $1/g_2 = r'_2$ if $Y'_b = 1/R'_b \approx 0$ is satisfied. In addition, the corresponding capacitances are the same, i.e., $C'_{s2} = C_{p2} = C'_{bs}C'_{bd}/(C'_{bs}+C'_{bd})$. Therefore, the result is reasonable. The parallel combination of $Z_{{\rm out},\,i1}$ and $C'_{s2}$, defined as $Z'_{{\rm out},\,i1}$, is still a series *RC* circuit, but with a smaller resistance $r'_1$ equal to $r_1\cdot[C_{s1}/(C_{s1}+C'_{s2})]^2$ and a larger capacitance $C'_{s1}$ equal to $C_{s1}+C'_{s2}$. Therefore, $Z_{{\rm out},\,i}$ can be represented by a parallel combination of $r'_2$ and $Z'_{{\rm out},\,i1}$. $R'_2 = (C'_{bs}+C'_{bd})/(g'_{mb}C'_{bd})$ only distorts the shape of $S_{22}$, which means changing the starting point of $S_{22}$ on the real axis from the open-circuit point to a point where the resistance approximately equals to $r'_2$. That is, at low frequencies when $R'_b \gg 1/|j\omega C'_{bs}|$

$$
\begin{aligned}
Z_{{\rm out},\,i} &= Z_{{\rm out},\,i1}\Big\|Z_{{\rm out},\,i2} \\
&\approx \left\{\left(\frac{Z_{O1}}{1+g'_mZ_{O1}}+\frac{g'_m}{(Y_{O1}+g'_m)^2}\cdot\frac{C'_{\rm gs}}{C'_{\rm gd}}\right)\right. \\
&\quad\cdot\left(\frac{(1+g'_mZ_{O1})C'_{\rm gd}}{(1+g'_mZ_{O1})C'_{\rm gd}+C'_{bd}C'_{bs}/(C'_{bd}+C'_{bs})}\right)^2 \\
&\quad\left.+\frac{1}{j\omega\left[(1+g'_mZ_{O1})C'_{\rm gd}+C'_{bd}C'_{bs}/(C'_{bd}+C'_{bs})\right]}\right\} \\
&\quad\cdot\left\|\left(\frac{(C'_{bs}+C'_{bd})}{g'_{mb}C'_{bd}}\right)\right. \\
&\approx \left[r_1\cdot\left(\frac{C_{s1}}{C_{s1}+C'_{s2}}\right)^2+\frac{1}{j\omega(C_{s1}+C'_{s2})}\right]\Big\|(r'_2) \\
&\approx \left(r'_1+\frac{1}{j\omega C'_{s1}}\right)\Big\|(r'_2). \qquad (13)
\end{aligned}
$$

To sum up, from the theoretical perspective, the effect of $R'_b$ on the kink phenomenon of the scattering parameter $S_{22}$ based on (5) and (10) is shown in Fig. 2. First, if $R'_b$ is small, then from (11) and (12), $r$ increases and $g$ decreases with the increase of $R'_b$. Hence, the kink point moves to a new interception point of a larger constant $r$ circle and a smaller constant $g$ circle at a smaller frequency, and the kink phenomenon becomes more prominent. Second, if $R'_b$ is within a middle range (approximately $10^2$ to $10^4$ $\Omega$), then from (11)–(13), an additional low-frequency kink point (approximately 1 GHz) can be observed. However, the additional kink point disappears when $R'_b \gg 1/|j\omega C'_{bs}|$ holds at low frequencies. This is because the starting point of $S_{22}$ on the real axis changes from the open-circuit point to a point where the resistance approaches $r'_2 = (C'_{bs}+C'_{bd})/(g'_{mb}C'_{bd})$. According to the above discussions, two types of kinks of the scattering parameter $S_{22}$ can be defined. The type-I kink is defined as the higher frequency kink (>5 GHz) that appears approximately at the interception point of the "shifted" constant $r$ circle (or constant $r$ circle) and the constant $g$ circle, while the type-II kink is the lower frequency kink (approximately 1 GHz) that appears approximately at the interception point of the constant $r$ circle and the "shifted" constant $r$ circle.

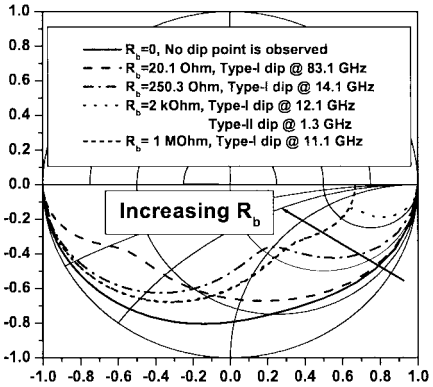


Fig. 2. Effect of substrate resistance ($R_b$) on the kink phenomenon of scattering parameter $S_{22}$ of RF MOSFETs.

## III. Experimental Results and Discussions

In order to explore the influence of the substrate resistance on the kink phenomenon of the scattering parameter $S_{22}$ of deep-submicrometer RF MOSFETs in real cases, we applied (1)–(9) to three 0.25-$\mu$m-gate nMOSFETs with different substrate resistances to calculate their $S$-parameters. The layout (gate length of 0.25 $\mu$m, and gatewidth of 80 $\mu$m, which were divided into eight fingers) and fabrication processes (super steep retrograde (SSR) indium channel, gate oxide thickness of 48 Å, etc.) of the three nMOSFETs were identical. In addition, the three nMOSFETs were fabricated at the same time. The only difference between them was the silicon wafers on which they were fabricated. As a result, the extracted substrate resistance of the three nMOSFETs turned out to be 20.1, 250.3, and 2000 $\Omega$, respectively.

The effect of the inductors in Fig. 1(a), which we neglected previously in Sections II and III, can be included by replacing $R_g$, $R_s$, $R_d$, and $R_b$ with $R_g+j\omega L_g$, $R_s+j\omega L_s$, $R_d+j\omega L_d$, and $R_b+j\omega L_b$, respectively. Excellent agreement between the calculated values and experimental data can be found, as shown in Fig. 3(a)–(c). Note that there is no visible kink phenomenon from the experimental data in Fig. 3(a). This is because the experimental data are collected at frequencies no more than 20 GHz. The reason why the kink phenomenon appears at frequencies higher than 20 GHz is because both the substrate resistance (20.1 $\Omega$) and gatewidth (80 $\mu$m) of the nMOSFET are too small. The kink phenomenon becomes more and more promi-

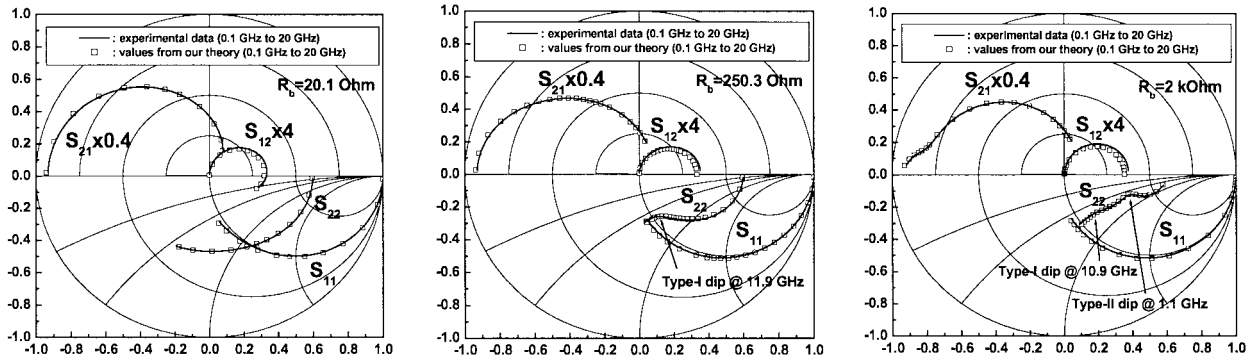


(a) (b) (c)

Fig. 3. Comparison of the experimental and calculated $S$-parameters of 0.25-$\mu$m-gate Si nMOSFETs with gatewidth of 80 $\mu$m and substrate resistance of: (a) 20.1, (b) 250.3, and (c) 2000 $\Omega$.

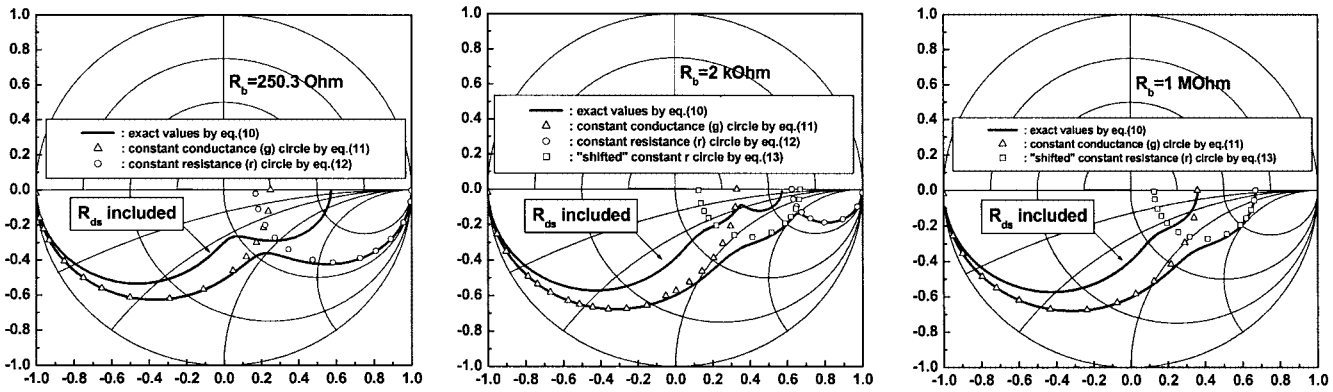


(a) (b) (c)

Fig. 4. Calculated $S_{22}$ at $R_b$ of: (a) 250.3 $\Omega$, (b) 2 k$\Omega$, and (c) 1 M$\Omega$. Note that $R'_{\rm ds}$ (or $R_{\rm ds}$) only changes the starting point of $S_{22}$ without affecting the appearance of the kink phenomenon.

nent at lower frequencies when the device's transconductance (or total gatewidth) increases, as demonstrated experimentally and theoretically in [2]. In addition, the kink phenomenon also becomes more and more prominent when the substrate resistance increases, as demonstrated experimentally by Hjelmgren and Litwin [1] and our experimental results in Fig. 3(b) and (c). The reason for the enhancement will be made clear in the following discussion.

The trends predicted by (11)–(13) have been verified in Fig. 4(a)–(c), where the data points have been calculated from (10)–(13). As can be seen from Fig. 4(a), under the condition of low substrate resistance equal to 250.3 $\Omega$, the intrinsic output impedance indeed follows a constant $r$ circle at low frequencies and then a constant $g$ circle at high frequencies. The kink phenomenon of $S_{22}$ of the nMOSFET in Fig. 3(b) belongs to the type-I kink because its substrate resistance (250.3 $\Omega$) is not high, gatewidth (80 $\mu$m) is small, and the frequency at which the kink occurs is high. The simulated kink in [1, Fig. 4] also belongs to the type-I kink, but the experimental kink in [1, Fig. 1] belongs to the type-II kink. Hjelmgren and Litwin seemed to regard these two types of kinks as the same, which is problematic.

Moreover, as can be seen from Fig. 4(b), under the condition of higher substrate resistance (2000 $\Omega$), the intrinsic output impedance first follows a constant $r$ circle, then a "shifted" constant $r$ circle at low frequencies, and then a constant $g$ circle at high frequencies. It is this inherent triple characteristic of the intrinsic output impedance (or admittance) that causes the appearance of the double-kink phenomenon of $S_{22}$ in a Smith chart, as shown in Fig. 3(c). Besides, as can be seen from Fig. 4(c), under the condition of a very high substrate resistance, which is generally greater than $10^6$ $\Omega$, the intrinsic output impedance follows a "shifted" constant $r$ circle at low frequencies and then a constant $g$ circle at high frequencies. Therefore, only the type-I kink exists. What is also shown in Fig. 4(a)–(c) is the effect of $R'_{\rm ds}$ (or $R_{\rm ds}$). Basically, $R'_{\rm ds}$ only changes the starting point of $S_{22}$ on the real axis either from the open-circuit point to a point where the resistance approaches $R'_{\rm ds}$ [see Fig. 4(a) and (b)] or from a point where the resistance approaches $r'_2 = (C'_{bs} + C'_{bd})/(g'_{mb}C'_{bd})$ to a point where the resistance approaches $r''_2 = R'_{\rm ds}||r'_2$ [see Fig. 4(c)], i.e., $R'_{\rm ds}$ only distorts the shape of $S_{22}$ without impeding the appearance of the kink phenomenon.

According to the previous discussions, we are able to explain the experimental data shown in Fig. 3(a)–(c). Obviously, if the substrate resistance of a MOSFET increases, we predict that the kink phenomenon should become more visible, i.e., the type-I kink point appears at lower frequencies. In addition, the type-II kink should appear in MOSFETs when the substrate resistance is within a middle range (approximately $10^2$–$10^4$ $\Omega$), which is indeed the case, as shown in Fig. 3(a)–(c), where the substrate resistance of 0.25-$\mu$m-gate nMOSFETs increased from 20.1 to 250.3 to 2000 $\Omega$, and $S_{22}$ was calculated by (1)–(9) with all the

extrinsic elements taken into account. Note that the calculated values we obtained are almost identical with the experimental data, as shown in Fig. 3(a)–(c). The calculated values of the other three $S$-parameters ($S_{11}$, $S_{21}$, and $S_{12}$) also agree with the experimental data very well and, thus, can justify this approach.

In conclusion, it is the inherent ambivalent characteristic (first follows a constant $r$ circle at low frequencies and then a constant $g$ circle at high frequencies) or triple characteristic (first follows a constant $r$ circle, then a "shifted" constant $r$ circle at low frequencies, and then a constant $g$ circle at high frequencies) of the output impedance that causes the appearance of the kink phenomenon of $S_{22}$ in a Smith chart, i.e., the "anomalous kink phenomenon" is a "normal behave" of $S_{22}$. From the point-of-view of device physics, the appearance of the kink phenomenon has nothing to do with any nonideal characteristics due to device defects or trapping of carriers. Actually, it results from the interaction of $C_{\rm gs}$, $C_{\rm gd}$, $C_{\rm ds}$, $g_m$, $C_{bs}$, $C_{bd}$, $g_{mb}$, and $R_b$, etc. If any of the previous terms results in an increase of $r$ and decrease of $g$, then the kink phenomenon will become more prominent. As shown in this paper and [1] and [2], an increase of device width or substrate resistance, corresponding to an increase of $r$ and decrease of $g$, makes the kink phenomenon more visible.

## IV. Conclusions

In this paper, a theory based on dual-feedback circuit methodology for the three-terminal FETs proposed by Lu *et al.* has been further applied to four-terminal RF MOSFETs in order to account for the effect of substrate resistance. The results have shown that, at low frequencies, the output impedance intrinsically behaves like a series *RC* circuit (for low substrate resistance) or a "shifted" series *RC* circuit (for very high substrate resistance), while at high frequencies, the output impedance intrinsically behaves like a parallel *RC* circuit. It is this inherent triple characteristic of the output impedance that causes the double-kink phenomenon, which has been experimentally demonstrated in this paper for the first time. Besides, the triple characteristic of the output impedance can also explain all the measured and simulated kink phenomena of $S_{22}$ reported in [1] and [2]. That is to say, the type-I kink, which occurs at higher frequencies, can be caused by either large substrate resistance [1] or large transconductance [2], while the type-II kink, which occurs at lower frequencies, can be caused by substrate resistance within a middle range (approximately $10^2$–$10^4$ $\Omega$) [1]. This study enables RF engineers to understand the behaviors of $S$-parameters more deeply, and is helpful for them in creating a fully scalable CMOS model for system-on-chip (SOC) applications.

## References


[1] H. Hjelmgren and A. Litwin, "Small-signal substrate resistance effect in RF CMOS identified through device simulations," *IEEE Trans. Electron Devices*, vol. 48, pp. 397–399, Feb. 2001.

[2] S.-S. Lu, C. Meng, T.-W. Chen, and H.-C. Chen, "The origin of the kink phenomenon of transistor scattering parameter $S_{22}$," *IEEE Trans. Microwave Theory Tech.*, vol. 49, pp. 333–340, Feb. 2001.

[3] H. Y. Tu, Y. S. Lin, P. Y. Chen, and S. S. Lu, "An analysis of the anomalous dip in scattering parameter $S_{22}$ of InGaP/GaAs heterojunction bipolar transistors (HBTs)," *IEEE Trans. Electron Devices*, vol. 49, pp. 1831–1833, Oct. 2002.

[4] F. X. Pengg, "Direct parameter extraction on RF-CMOS," in *IEEE Radio Frequency Integrated Circuits Symp.*, 2002, pp. 355–358.

[5] S. Lee, H. K. Yu, C. S. Kim, J. G. Koo, and K. S. Nam, "A novel approach to extracting small-signal model parameters of silicon MOSFET's," *IEEE Microwave Guided Wave Lett.*, vol. 7, pp. 75–77, Mar. 1997.

[6] P. R. Gray and R. G. Meyer, *Analysis and Design of Analog Integrated Circuits*. New York: Wiley, 1993, pp. 579–584.



**Yo-Sheng Lin** (M'02) was born in Puli, Taiwan, R.O.C., on October 10, 1969. He received the Ph.D. degree in electrical engineering from the National Taiwan University, Taipei, Taiwan, R.O.C., in 1997. His doctoral dissertation concerned the fabrication and study of GaInP/InGaAs/GaAs doped-channel FETs and their applications on monolithic microwave integrated circuits (MMICs).

In 1997, he joined the Taiwan Semiconductor Manufacturing Company (TSMC) as a Principle Engineer for 0.35/0.32 DRAM and 0.25 embedded DRAM technology developments in the Integration Department of Fab-IV. In 2000, he was responsible for 0.18/0.15/0.13-mm CMOS low-power device technology development with the Department of Device Technology and Modeling, Research and Development, and became a Technical Manager in 2001. He is currently an Assistant Professor with the Department of Electrical Engineering, National Chi-Nan University, Puli, Taiwan, R.O.C. His current research interests are the areas of characterization and modeling of RF active and passive devices, and radio-frequency integrated circuits (RFICs)/MMICs.



**Shey-Shi Lu** (S'89–M'91–SM'99) was born in Taipei, Taiwan, R.O.C., on October 12, 1962. He received the B.S. degree from the National Taiwan University, Taiwan, R.O.C., in 1985, the M.S. degree from Cornell University, Ithaca, NY, in 1988, and the Ph.D. degree from the University of Minnesota at Minneapolis–St. Paul, in 1991, all in electrical engineering. His M.S. thesis concerned the planar doped barrier hot electron transistor, while his doctoral dissertation concerned the uniaxial stress effect on AlGaAs/GaAs quantum well/barrier structures.

In August 1991, he joined the Department of Electrical Engineering, National Taiwan University, where he is currently a Professor. His current research interests are the areas of radio-frequency integrated circuits (RFICs)/MMICs and micromachined RF components.